1-1-2018

Computer-aided design of human sialyltransferase inhibitors of hST8Sia III

Christopher Dobie
University of Wollongong, cd959@uowmail.edu.au

Andrew Montgomery
University of Wollongong, apm977@uowmail.edu.au

Remi Szabo
University of Wollongong, rs424@uowmail.edu.au

Danielle Skropeta
University of Wollongong, skropeta@uow.edu.au

Haibo Yu
University of Wollongong, hyu@uow.edu.au

Computer-aided design of human sialyltransferase inhibitors of hST8Sia III

Abstract

Sialyltransferase (ST) upregulation and the resultant hypersialylation of tumour cell surfaces is an established hallmark of many cancers including lung, breast, ovarian, pancreatic and prostate cancer. The role of ST enzymes in tumour cell growth and metastasis, as well as links to multi-drug resistance, has seen ST inhibition emerge as a target for potential antimetastatic cancer treatments. The most potent of these reported inhibitors are transition-state analogues. Although there are several examples of these in the literature, many have suspected poor pharmacokinetic properties and are not readily synthetically accessible. A proposed solution to these problems is the use of a neutral carbamate or 1,2,3-triazole linker instead of the more commonly used phosphodiester linker, and replacing the traditionally utilised cytidine nucleotide with uridine. Another issue in this area is the paucity of structural information of human ST enzymes. However, in late 2015 the structure of human ST8Sia III was reported (only the second human ST described so far), creating the opportunity for structure-based design of selective ST8 inhibitors for the first time. Herein, molecular docking and molecular dynamics simulations with the newly published crystal structure of hST8Sia III were performed for the first time with selected ST transition state analogues. Simulations showed that these compounds could participate in many of the key interactions common with the natural donor and acceptor substrates, and reveals some key insights into the synthesis of potentially selective ST inhibitors.

Disciplines

Medicine and Health Sciences

Publication Details

Dobie, C., Montgomery, A. P., Szabo, R., Skropeta, D. & Yu, H. (2018). Computer-aided design of human sialyltransferase inhibitors of hST8Sia III. Journal of Molecular Recognition, 31 (2), e2684-1-e2684-11.

Computer-aided design of human sialyltransferase inhibitors of hST8Sia III

Short title: Computer-Aided Design of Human ST8Sia III Inhibitors

Authors: Christopher Dobie,[a] Andrew P Montgomery,[a] Rémi Szabo,[a] Danielle Skropeta,[a,b,c] and Haibo Yu[a,b,c]

Affiliations: [a] School of Chemistry, Faculty of Science, Medicine and Health, University of Wollongong, Wollongong NSW 2522, Australia

[b] Centre for Medical and Molecular Bioscience, University of Wollongong, Wollongong NSW 2522, Australia

[c] Illawarra Health and Medical Research Institute, University of Wollongong, Wollongong NSW 2522, Australia

Author to Check Proofs:

Haibo Yu, School of Chemistry, University of Wollongong, NSW 2522, Australia.

Email: hyu@uow.edu.au

Phone: +61 2 4221 4235

Fax: +61 2 4221 4287

Abstract: Sialyltransferase (ST) upregulation and the resultant hypersialylation of tumour cell surfaces is an established hallmark of many cancers including lung, breast, ovarian, pancreatic and prostate cancer. The role of ST enzymes in tumour cell growth and metastasis, as well as links to multi-drug resistance, has seen ST inhibition emerge as a target for potential antimetastatic cancer treatments. The most potent of these reported inhibitors are transition-state analogues. Although there are several examples of these in the literature, many have

suspected poor pharmacokinetic properties and are not readily synthetically accessible. A proposed solution to these problems is the use of a neutral carbamate or 1,2,3-triazole linker instead of the more commonly used phosphodiester linker, and replacing the traditionally utilised cytidine nucleotide with uridine. Another issue in this area is the paucity of structural information of human ST enzymes. However, in late 2015 the structure of human ST8Sia III was reported (only the second human ST described so far), creating the opportunity for structure-based design of selective ST8 inhibitors for the first time. Herein, molecular docking and molecular dynamics simulations with the newly published crystal structure of hST8Sia III were performed for the first time with selected ST transition state analogues. Simulations showed that these compounds could participate in many of the key interactions common with the natural donor and acceptor substrates, and reveals some key insights into the synthesis of potentially selective ST inhibitors.

Keywords: sialyltransferase; inhibitors; molecular docking; molecular dynamics simulations; ST8Sia; transition-state analogues; metastasis

INTRODUCTION

Hyperglycosylation of tumour cells, in particular hypersialylation due to overexpression of sialyltransferases (STs) is a well-established hallmark of cancer, which makes the development of selective inhibitors a vital area of inquiry in cancer treatment.[1-3] STs are enzymes of the glycosyltransferase family that catalyse the formation of an α-glycosidic bond between the C2 atom of a sialic acid (*N*-acetylneuraminic acid, or Neu5Ac) and a hydroxyl group of a glycan acceptor.[4-5] In humans all, STs utilise the common donor cytidine monophosphate Neu5Ac (CMP-Neu5Ac). There are 20 different human sialyltransferase enzymes which catalyse the biosynthesis of cell surface glycoconjugates.[6-8] These subtypes are each expressed in different cell types, potentially allowing for specific targeting of the enzymes, which are overexpressed in many forms of cancer such as colorectal,[9-10] breast,[11] and pancreatic cancer.[12] Selective targeting of specific ST subtypes has been shown to be crucial in order to avoid off-target effects such as liver and kidney dysfunction (in mice), which has been observed for global inhibitors.[13]

STs are named according to the position of the glycosidic bond that they catalyse, and the glycan acceptor to which the sialic acid is bound. In humans four families of STs exist, which catalyse the formation of an α-glycosidic linkage between the 2′ position of the sialic acid donor and the 3′, 6′, and 8′ hydroxyl group of the glycan acceptor.[5] These are classified as ST3, ST6, and ST8 respectively, followed by the sugar molecule to which they form the linkage (e.g. Gal, GalNAc, Sia). The ST8Sia subfamily (of which there are six members) catalyse an α-2,8 linkage between two sialic acids, while having different specificities for the length of the sialic acid acceptor. Within this subfamily, ST8Sia III is the only member which shows a specificity for oligosialic acids.[14]

ST8Sia III is a membrane-bound enzyme fixed to the Golgi apparatus, with the catalytic domain located in the lumen (Figure 1).[4] In the literature, ST structures have been resolved

for nine species of bacteria[4,15-22] and only four different mammalian structures.[7,14,23-24] The porcine ST3Gal I (pST3Gal I)[23] was resolved in 2009, both rat[24] and human[7] ST6Gal I (rST6Gal I and hST6Gal I respectively) in 2013, and most recently in 2015, the structure of human ST8Sia III (hST8Sia III)[14] has been determined, co-crystallised with various substrates, such as 5'-O-[(R)-[(S)-[3-(acetylamino)phenyl](phosphono)methoxy](hydroxy) phosphoryl] cytidine (55T).[25] These new structures allow for comparisons to be made between binding sites, to investigate potential avenues for selective inhibitor design.

Previous studies into ST inhibitors have identified transition-state analogues as the most potent reported to date.[2,26-28] These compounds mimic the planar oxocarbenium-like transition-state of the ST mechanism, using the sialic acid donor CMP-Neu5Ac (**1**) as a starting point (Figure 2). Some of the earliest compounds (such as **2**, K_i = 350 nM; α-2,6-ST) added a planar bond to the sialic acid mimic, and replaced the carboxylate group with a phosphonate, giving markedly improved activity.[29] Replacing the sialic acid mimic with a simpler *meta*-phenoxy aromatic system, resulted in a further increase in potency giving one of the most potent human ST inhibitors to date, compound **3** (K_i = 19 nM; hST6Gal I).[30-31] However, there are perceived pharmacokinetic issues with this compound, as it is believed that the phosphodiester linkage may be susceptible to cleavage by phosphatases *in vivo* (and potentially cleavage by the STs themselves, as the CMP leaving group is still present), rendering the compound inactive.[32] To address this issue, it has been proposed that replacing the charged phosphodiester linkage with a neutral carbamate (**4**), or 1,2,3-triazole (**6**), group could improve drug-likeness of the inhibitors.[33-34] Another potential alteration to the lead compound **3** is the exchange of the cytidine moiety with a uridine (**5** and **7**), in order to aid synthetic accessibility and to probe potential selectivity between ST subtypes.

The aim of this study is to develop an understanding of the specificities of ST8Sia III by computational analysis of ligand-protein interactions, using compounds **4**-**7** as a starting point.

With comparison with previous work on ST6Gal I,[33,35] this will inform the rational design of potent and selective ST inhibitors with favourable pharmacokinetic properties.

METHODS

General Docking Procedure: Potential inhibitors (**4-33**) were docked into the binding site of one monomer of the hST8Sia III crystal structure (PDB ID:5CXY)[25] with AutoDock Vina (AD-Vina) version 1.1.2.[36] Receptor structures were prepared for docking using AutoDockTools (ADT) version 4.2.6.[37] The three-dimensional structure of the inhibitors were prepared utilising ChemDraw 15.0 and Avogadro v1.1.1.[38] ADT was used to assign both rigid and rotatable bonds and to remove non-polar hydrogens. Docking was performed for a box of 30 Å × 30 Å × 30 Å centred at the active site. The dimension was chosen to ensure it was large enough to cover all key active site residues identified in hST8Sia III by Volkers *et al*.[14] and to accommodate the largest ligand investigated herein. The docking procedure was validated by re-docking to replicate the crystallographically determined hST8Sia III-55T complex (Figure 1). The receptor is treated as rigid and no explicit waters have been included. The top ranked models for each compound tested based on the binding affinities calculated by AD-Vina were evaluated based upon comparison to the position of 55T in the crystal structure of hST8Sia III (Figure 1)[25] with VMD v1.9.2.[39] Ranking of inhibitors according to docking results was further validated by docking compounds with known inhibition values from biological testing (unpublished data – personal communication, Gerardy-Schahn, R). Statistical analysis was undertaken on the calculated binding affinities for each compound to determine if they were statistically different from one another, using a two-tailed students *t*-test. Results were deemed significant for $P < 0.05$.

Molecular Dynamics Simulations: Molecular systems for MD simulations were prepared using VMD v1.9.2.[39] For simulations involving a ligand, the ligand was docked into the crystal structure using AD Vina according to the method above (See Table 1 for a description

of the simulations carried out). The simulated ligands varied in the linker used; carbamate (CAR), 1,2,3-triazole (TRI), and phosphodiester (LEAD). The system was prepared by solvating the protein crystal structure in a water box, with a space of at least 9.0 Å from each side of the surface of the protein. The water box was also ionised with NaCl to a concentration of 0.15 mol/L. MD simulation was carried out with NAMD 2.11,[40] and the force fields used were the CHARMM PARAM36 force field for the protein,[41] and force field parameters specific to the ligands which were generated by Montgomery *et al.*[33] using cGenFF[42] and optimised using the GAAMP method.[43-44] The systems were simulated in periodic boundary conditions using the Langevin algorithm for maintaining the temperature at 298.15 K, and the Langevin Piston Nose-Hoover method to keep the pressure constant at 1.0 bar.[45-46] Van der Waals forces were treated with a cut-off distance of 12.0 Å with a smoothening function between 10.0 and 12.0 Å , while electrostatic interactions were calculated using the Particle mesh Ewald method.[47] Covalent bonds involving hydrogen had their rigidity maintained by the RATTLE algorithm.[48] The integration time step was set to 1.0, 2.0, and 4.0 fs for bonded, non-bonded, and long range electrostatic interactions respectively. Triplicated equilibrium simulations were undertaken for each system, for the first 10 ns with a harmonic restraint placed upon the Cα atoms of the protein with a decreasing force constant over the 10 ns. The force was halved every nanosecond of simulation, starting from 32.0 kcal/mol/Å^2 until the force constant reached 1.0 kcal/mol/Å^2, which was applied for the remainder of the first 10 ns of simulation. The simulations were then run for a further 90 ns without any restraints, with snapshots saved every picosecond (1000 steps). In total, 1.9 microseconds of simulations were carried out.

RMSD and RMSF Analysis: In order to analyse the structural changes in the protein over the course of the simulations, root-mean-square deviation (RMSD) of protein Cα atoms and

ligands, and root-mean-square fluctuation (RMSF) of Cα atoms with respect to the starting structure were calculated for the course of each simulation, using VMD v1.9.2.[39]

ST8Sia III-ligand Interaction Analysis: For the MD simulations performed, key interactions were analysed using CHARMM v.38a1,[49] according to specific criteria. Hydrogen bonds were defined by a maximum donor-acceptor distance of 3.0 Å, and minimum donor-hydrogen-acceptor angle of 120°, with minimum 10% occupancy. Water-bridged hydrogen bonds were defined via the same variables, with a minimum of 30 % occupancy. Hydrophobic contacts were defined by a maximum distance between hydrophobic atom pairs of 4.0 Å, with minimum 10% occupancy.

RESULTS AND DISCUSSION

Investigation of hST8Sia III crystal structure

The crystal structure of hST8Sia III was recently published by Volkers *et al*.[14] in 2015. In the study, hST8Sia III was crystallised as an apo structure, and with three substrates; cytidine diphosphate (CDP), cytidine triphosphate (CTP) and the natural donor mimic CMP-3FNeu5Ac (along with the acceptor Sia-6S-LacNAc). It was also demonstrated that hST8Sia III adopts a dimeric structure in solution, which is believed to contribute to stabilisation and membrane tethering, rather than a change in activity.[14] This is contrary to the ST8Sia II and IV subtypes, which appear to be monomeric.[14] There was a flexible loop observed in hST8Sia III over the active site between residues Lys341-His354, which was not fully resolved in all but one crystal structure (hST8Sia III co-crystallised with CDP). This indicates that the loop is highly disordered, which is proposed to adopt a number of conformational states. There is also a hydrophobic patch above the donor binding site (Lys349-Ser353), which is believed to play a role in acceptor specificity within the ST8Sia enzyme family.[14] The His354 residue is believed to be a catalytic residue for ST8Sia III, and is observed interacting with the O8′ of the acceptor

sialic acid.[14] To date, there have been no computational studies performed on hST8Sia III for the purposes of inhibitor design and so herein is described the first of this type performed on this enzyme. A crystal structure was also released on the PDB by Volkers & coworkers in 2016 with ST8Sia III co-crystallised with 5'-O-[(R)-[(S)-[3-(acetylamino)phenyl](phosphono) methoxy](hydroxy)phosphoryl]cytidine (55T), which has a comparable structure to the lead ST inhibitor (**3**, Figure 2).[25] These recent developments indicate the potential for development of selective inhibitors, with the availability of multiple crystal structures of these human ST enzymes giving the opportunity for structure-based drug design for the first time.

Comparison between binding sites of pST3Gal I, hST6Gal I, and hST8Sia III

To gain an insight into the potential structural features of selective hST8Sia III inhibitors, structural alignment of three mammalian STs (pST3Gal I, hST6Gal I, and hST8Sia III) was performed using BIOVIA Discovery Studio Visualizer,[50] centred around the donor molecule binding pocket (Figure 3). It was observed that for both pST3Gal I (85 % homology to hST3Gal I) and hST8Sia III, there was a hydrophobic sub-pocket adjacent to the 2′ position on the ribose ring of the co-crystallised ligands (shown by the colour gradient in Figure 3). Hydrophobicity was calculated using the method of Kyte and Doolittle, which assigns a value to each amino acid based on its hydrophobicity.[51] These values then contribute to the averaged surface hydrophobicity. There is also a sub-pocket present in the hST6Gal I structure, although it was smaller than in the other two subtypes, and offset from the 2′ position. This indicates that pST3Gal I and hST8Sia III may tolerate inhibitors with substitutions on the 2′ position, while hST6Gal I will not, as has been shown experimentally.[2] It appears that the sub-pocket mentioned is also larger for pST3Gal I than for hST8Sia III, which could lead to further selectivity between the two (if hST3Gal I adopts the same binding pocket structure).

Stability and flexibility of the hST8Sia III-ligand complexes

The effects of ligand binding on the structural stability and flexibility of hST8Sia III over the course of the MD simulations were assessed. The RMSD of protein carbon alphas (Cα) for all simulations converged between 1.5 and 2.5 Å (Figure S1-S7), indicating that there was no significant change in the overall structure of the protein. The heavy atom positional RMSD of the ligand in the carbamate (CAR) simulations converged between 1.5 and 2.5 Å (Figures S8 and S9), the phosphodiester (LEAD) simulations converged between 2.0 and 2.5 Å (Figures S10 and S11), triazole (TRI) simulations converged between 2.0 and 3.5 Å (Figures S12 and S13), except for one of the *(S)*-triazole (TRI_S) simulations, which stabilised at 1.5 Å. This indicates that the more flexible carbamate and phosphodiester linked compounds were better able to fit in the binding site of ST8Sia III and adopt a more stable conformation, as opposed to the more rigid triazole compound. In terms of the RMSF of the protein Cα atoms, all ligand-protein complex simulations exhibited lower RMSF values for the flexible loop from Lys341 to His354 than those observed for the apo simulation, which peaked at 3.5 Å (Figure 4). This effect is due to favourable ligand-protein interactions that serve to stabilise the loop. Of these simulations, the triazole complexes exhibited the smallest change in RMSF for the loop, which was between 1.5 and 3.5 Å (Figure S16). This may be due to the rigidity of the triazole linker, which necessitates additional movement by the protein to accommodate it.

Comparison of the binding modes of carbamate- and 1,2,3-triazole-linked inhibitors with hST8Sia III

Docking of potential inhibitors (**4-27**) of ST8Sia III and their phosphodiester equivalents (**3**, **28**-**38**) into snapshots (20 ns intervals from 0-100 ns) from the carbamate simulation (CAR_R1) was undertaken (results from statistical analysis in Tables S1-S17). The compounds were chosen based on a previous study by Montgomery *et al*,[33] to assess their difference in binding against hST6Gal I. Statistical analysis was performed to determine if the differences between

the calculated binding affinities were significant. The analysis gave a wide range of *p*-values, ranging from 7.16×10^{-6} to 1 across different comparison pairs.

Across all compounds analysed, there was no significant difference between the binding affinities of the *R* and *S* stereoisomers of the same compounds. Although this is counterintuitive, this result correlates with previously observed experimental and computational results for other STs.[30,33] This appears to be due to the relatively larger space available in the binding site, while still allowing for the ligand to interact with residues that are key for binding.

There was also no significant difference in the binding affinities of cytidine (**3**, **4**, **6**, **8-12**, **18-22**, **28-32**) and uridine (**5**, **7**, **13-17**, **23-27**, **33-38**) derivatives of the same compounds (Table 2, 3 and 4). This suggests that there may be no specificity observed in hST8Sia III for cytidine-based compounds over uridine based. This could open a door to selective inhibitor design, as the cytidine moiety is believed to be crucial to the activity of hST6Gal I inhibitors (although there is experimental evidence that hST3Gal I could also accept uridine derivatives).[2,7] The two derivatives also exhibited near-identical predicted binding modes (Figure 5A). This result suggests that uridine derivatives of ST inhibitors may be selective against ST6Gal I, and that they may be a viable (and more synthetically accessible) alternative than their cytidine equivalents.

The phosphodiester-linked compounds tested did not show any significant differences in binding affinity compared to their carbamate- and 1,2,3-triazole-linked equivalents, suggesting that the use of carbamate and 1,2,3-triazole linkers do not have any major effect on the binding mode of these potential ST inhibitors.

While not statistically significant in the majority of cases, it was noted that each 1,2,3-triazole-linked derivative produced a greater binding affinity than its carbamate-linked equivalent (with

the single exception of ***(R)*-11** exhibiting a higher average binding affinity than ***(R)*-21**, which was greater by 0.1 kcal/mol, a difference which was not statistically significant). This result indicates that the differences in binding affinities of compounds with 1,2,3-triazole- and carbamate-linkers are not significant and in fact comparable to one another.

In terms of the binding modes of the potential inhibitors, it was noted that there were two main binding pockets towards which the sialyl mimic segment of the inhibitor was directed, with a third conformation being less frequent (demonstrated in Figure 5B). This indicates that there is a reasonable degree of flexibility in the structure of potential inhibitors in the region traditionally occupied by the sialyl mimic.

Effect of 2′ substitution on inhibitor binding

To probe the effect on binding of substitutions at the 2′ position of ST inhibitors and to what degree they may be accommodated by the binding pocket of hST8Sia III, docking was performed with uridine-based carbamate derivatives (**5**, **39-44**, Table 5). It was found that there was no significant difference between the calculated binding affinities of the compounds with substitutions up to the size of a propoxy group and the non-substituted compound ***(R)*-5** (Table 5). Inhibitors with substitutions larger than this (such as a benzyl group) were not able to adopt a suitable binding conformation, indicating a limit to the size tolerance of the sub-pocket.

Analysis of binding interactions between hST8Sia III and potential inhibitors

Analyses were performed on the protein-ligand complex MD simulations as part of this work to determine the consistent hydrogen bonds and hydrophobic contacts between the ligands and protein. These interactions were then compared to the non-bonded interactions described by Volkers *et al.*,[14] identified in the X-ray crystal structures of hST8Sia III with donor and acceptor analogues (Figure 6). When comparing the protein-ligand interactions observed in the

MD simulations, there was a greater similarity between the carbamate (CAR) and phosphodiester (LEAD) simulations than with the triazole (TRI) simulations.

The carbamate (CAR) and phosphodiester (LEAD) simulations were found to more closely mimic the interactions observed in the hST8Sia III crystal structure complex, compared to the TRI simulations. This may be due to the increased rigidity of the triazole linker, meaning that the ligand was less able to adopt a conformation which matched the donor and acceptor analogues. Key similarities between the carbamate (CAR) and phosphodiester (LEAD) simulations are shown in Figure 7. Two residues that had consistent interactions in both the simulations and the crystal structure include Asn167 and Thr301. The residue Asn167 was observed interacting with the phosphate group of the donor analogue, while in the carbamate (CAR) and phosphodiester (LEAD) simulations it was involved in hydrogen bonding with the cytidine N6 and ribose oxygen. In the case of the *R* stereoisomers, Asn167 also participated in hydrogen bonding with the carbamate and phosphodiester linkers, which indicate that they are effectively mimicking the phosphate of the donor analogue. In the crystal structure, Thr301 was observed interacting with the carboxylate group of CMP-3FNeu5Ac, where as in the MD simulations it was interacting with the linker (in the case of the carbamate compounds), the 3′-hydroxyl, and in the phosphodiester (LEAD) simulations, the phosphonate group, which is intended to be an analogue of the carboxylate. One key difference that was observed across the stereoisomers of the carbamate (CAR) and phosphodiester (LEAD) simulations were that the linker at the *R* stereoisomers was interacting with the Asn190 residue, while the linker of the *S* stereoisomers was interacting with His337 via a water-bridged hydrogen bond. Both residues are noted to interact with the phosphonate group of CMP-3FNeu5Ac in the crystal structure. This expands upon previous work by Montgomery *et al.*[33] on hST6Gal I, and indicates that the carbamate linker is effective at mimicking the phosphodiester linker of the earlier ST inhibitors.

Other hydrogen bonding interactions which were consistent between both the *R* and *S* stereoisomers which were not explicitly noted by Volkers *et al.*[14] These include the residues Tyr336, Trp322, and Ser168, which all had hydrogen-bonding interactions with the cytidine moiety, while Gly302 had interactions with both 2′ and 3′ hydroxyl groups. These residues appear to be important in helping to orient the nucleotide fragment of the inhibitors in the active site, while also allowing the sialyl mimic of the inhibitor to adopt a more favourable conformation in the hydrophobic pocket of the active site.

In terms of hydrophobic contacts observed over the course of the MD simulations for the carbamate (CAR) and phosphodiester (LEAD) ligands, there were five residues which had conserved interactions across *R* and *S* stereoisomers of both ligands (Figure 8). These residues include Phe321, Tyr336, His337, His354, and Leu356. It was interesting that there was only one conserved interaction with the aromatic region of the ligands, that being between the catalytic residue His354 and the aromatic sialyl mimic, when it occupies a large hydrophobic pocket, as observed by Volkers *et al.*[14] A potential explanation for this observation is that while occupancies for specific interactions were lower than 10 %, there is a large number of hydrophobic residues in that region, resulting in a wide variety of hydrophobic contacts being made throughout the simulations. Since His354 was observed in the crystal structure to interact (albeit via hydrogen bonding) with the sialyl acceptor, these results indicate that these potential inhibitors are effective at mimicking the planar transition-state of the ST mechanism.

While results from the triazole (TRI) simulations were less consistent with the crystal structure than those for the carbamate (CAR) and phosphodiester (LEAD) simulations, the protein-ligand interactions that were observed give an insight into inhibitor design for selective ST8Sia III inhibitors. Two hydrogen bonding interactions that were consistent with the hST8Sia III crystal structure were noted (Figure 9A), with Asn167 and Thr301 being the residues involved in binding to the cytidine oxygen and triazole linker, respectively.

Hydrophobic contacts for the triazole (TRI) simulations were consistent with the carbamate (CAR) and phosphodiester (LEAD) simulations for the cytidine moiety, with variations at the sialyl mimic (Figure 9B). The triazole (TRI) simulations exhibited more consistent hydrophobic interactions with the sialyl mimic, with the residues Pro246, Phe249, and Phe250 (which interacted with each of the aromatic rings in the separate *R* and *S* simulations). The greater consistency in hydrophobic interactions with the sialyl mimic for the triazole (TRI) simulations as opposed to the carbamate (CAR) and phosphodiester (LEAD) could be due to the relative rigidity of the triazole linker. This would mean that the sialyl mimic is less mobile in the binding pocket, and more consistent interactions are observed when compared to the simulations with more flexible interactions.

Implications for the design of selective ST inhibitors

Previous work by our group has highlighted the suitability for carbamate and 1,2,3-triazole linkers as isosteres of the charged phosphodiester group of classical ST inhibitors, particularly for ST6Gal I.[33-34] The results found in this study show a similar observation for inhibitors of ST8Sia III, with comparable binding patterns and interactions observed (particularly for the carbamate-linked inhibitors). The results of this study showed no significant difference in the calculated binding affinity of inhibitors bearing a uridine or cytidine moiety, which provides support for the use of uridine as a nucleotide base for ST inhibitors, particularly for ST8Sia III. This could be a route for the synthesis of selective inhibitors if it is found that uridine derivatives have a lessened binding affinity for other ST subtypes such as ST6Gal I. Results from both docking and MD also indicate that there is little difference in the binding modes and interactions between *R* and *S* stereoisomers of the same inhibitor.

While there was little significant difference between the predicted binding affinities of the triazole and carbamate derivatives of the inhibitors analysed here, there was a trend of triazole compounds exhibiting a slightly higher binding affinity. Conclusive characterisation of such

effects will require rigorous binding free energy calculations. Additionally, and perhaps most importantly for the development of selective inhibitors, is the observation that the binding pocket of ST8Sia III can accommodate substitution at the 2′ position of ST inhibitors without a detrimental effect to their binding affinity. This is in contrast to ST6Gal I, which does not accommodate such substitutions.[2] These observations should be probed further and may yield promising results in the realm of selectivity, at the very least against ST6Gal I.

CONCLUSIONS:

Computational analysis of potential inhibitor binding was performed using the crystal structure of hST8SiaIII for the first time. A validated docking procedure was used to assess 42 distinct compounds and their stereoisomers. The results suggested that there was no significant difference in the predicted binding affinity of inhibitors bearing either a uridine or cytidine nucleotide moiety. Docking results also showed that there was no significant difference between the binding affinity of the *R* and *S* diastereomers of the proposed inhibitors. MD simulations determined that the proposed carbamate- and triazole-linked transition state analogues bound to the hST8Sia III active site in a similar conformation to the co-crystallised inhibitor analogue 55T, and the donor and acceptor analogues from the published crystal structures, while retaining some key interactions with the protein. This work provides a foundation for more rigorous characterisation of binding affinities and selectivities based on free energy calculations, which is currently underway. Furthermore, current studies also provide important insights for the synthetic and biological exploration of 2′-substituted carbamate and 1,2,3-triazole-linked ST inhibitors, which display a potential for selectivity.

ACKNOWLEDGEMENTS:

We wish to acknowledge the University of Wollongong and Illawarra Cancer Carers for a joint scholarship for C.D. We also acknowledge the Australian Government for an Australian

Research Council Future Fellow for H.Y. (FT110100034) and an Australian Government Research Training Program Award scholarship for A.P.M. We also wish to acknowledge Phil Clingan, Maxine Stewart and the Illawarra Cancer Carers for financial support. This research was in part supported under the Australian Research Council's Discovery Projects funding scheme (project number DP170101773). This research was undertaken with the assistance of resources provided at the NCI National Facility systems at the Australian National University through the National Computational Merit Allocation Scheme supported by the Australian Government.

REFERENCES:

1. Munkley, J.; Elliott, D. J., Hallmarks of glycosylation in cancer. *Oncotarget* **2016**, *7* (23), 35478-89 DOI: 10.18632/oncotarget.8155.
2. Szabo, R.; Skropeta, D., Advancement of Sialyltransferase Inhibitors: Therapeutic Challenges and Opportunities. *Med Res Rev* **2017**, *37*, 219-270 DOI: 10.1002/med.21407.
3. Büll, C.; Stoel, M. A.; den Brok, M. H.; Adema, G. J., Sialic Acids Sweeten a Tumor's Life. *Cancer Research* **2014**, *74* (12), 3199-3204 DOI: 10.1158/0008-5472.can-14-0728.
4. Li, Y.; Chen, X., Sialic Acid Metabolism and Sialyltransferases: Natural Functions and Applications. *Appl Microbiol Biotechnol* **2012**, *94* (4), 887-905 DOI: 10.1007/s00253-012-4040-1.
5. Lairson, L. L.; Henrissat, B.; Davies, G. J.; Withers, S. G., Glycosyltransferases: Structures, Functions, and Mechanisms. *Annu Rev Biochem* **2008**, *77* (1), 521-555 DOI: 10.1146/annurev.biochem.76.061005.092322.
6. Harduin-Lepers, A.; Vallejo-Ruiz, V.; Krzewinski-Recchi, M. A.; Samyn-Petit, B.; Julien, S.; Delannoy, P., The Human Sialyltransferase Family. *Biochimie* **2001**, *83* (8), 727-37 DOI: 10.1016/S0300-9084(01)01301-3.
7. Kuhn, B.; Benz, J.; Greif, M.; Engel, A. M.; Sobek, H.; Rudolph, M. G., The Structure of Human α-2,6-Sialyltransferase Reveals the Binding Mode of Complex Glycans. *Acta Crystallogr D Biol Crystallogr* **2013**, *69* (Pt 9), 1826-38 DOI: 10.1107/s0907444913015412.
8. Fernández-Suárez, X. M.; Rigden, D. J.; Galperin, M. Y., The 2014 Nucleic Acids Research Database Issue and an updated NAR online Molecular Biology Database Collection. *Nucleic Acids Res* **2014**, *42* (Database issue), D1-D6 DOI: 10.1093/nar/gkt1282.
9. Seales, E. C.; Jurado, G. A.; Brunson, B. A.; Wakefield, J. K.; Frost, A. R.; Bellis, S. L., Hypersialylation of β1 Integrins, Observed in Colon Adenocarcinoma, May Contribute to Cancer Progression by Up-Regulating Cell Motility. *Cancer Res* **2005**, *65* (11), 4645-52 DOI: 10.1158/0008-5472.can-04-3117.
10. Park, J.-J.; Lee, M., Increasing the α-2,6 Sialylation of Glycoproteins May Contribute to Metastatic Spread and Therapeutic Resistance in Colorectal Cancer. *Gut Liver* **2013**, *7* (6), 629-641 DOI: 10.5009/gnl.2013.7.6.629.

11. Bos, P. D.; Zhang, X. H.; Nadal, C.; Shu, W.; Gomis, R. R.; Nguyen, D. X.; Minn, A. J.; van de Vijver, M. J.; Gerald, W. L.; Foekens, J. A.; Massague, J., Genes that Mediate Breast Cancer Metastasis to the Brain. *Nature* **2009**, *459* (7249), 1005-9 DOI: 10.1038/nature08021.

12. Perez-Garay, M.; Arteta, B.; Llop, E.; Cobler, L.; Pages, L.; Ortiz, R.; Ferri, M. J.; de Bolos, C.; Figueras, J.; de Llorens, R.; Vidal-Vanaclocha, F.; Peracaula, R., α2,3-Sialyltransferase ST3Gal IV Promotes Migration and Metastasis in Pancreatic Adenocarcinoma Cells and Tends to be Highly Expressed in Pancreatic Adenocarcinoma Tissues. *Int J Biochem Cell Biol* **2013**, *45* (8), 1748-57 DOI: 10.1016/j.biocel.2013.05.015.

13. Macauley, M. S.; Arlian, B. M.; Rillahan, C. D.; Pang, P.-C.; Bortell, N.; Marcondes, M. C. G.; Haslam, S. M.; Dell, A.; Paulson, J. C., Systemic Blockade of Sialylation in Mice with a Global Inhibitor of Sialyltransferases. *J Biol Chem* **2014**, *289* (51), 35149-35158 DOI: 10.1074/jbc.M114.606517.

14. Volkers, G.; Worrall, L. J.; Kwan, D. H.; Yu, C. C.; Baumann, L.; Lameignere, E.; Wasney, G. A.; Scott, N. E.; Wakarchuk, W.; Foster, L. J.; Withers, S. G.; Strynadka, N. C., Structure of Human ST8SiaIII Sialyltransferase Provides Insight into Cell-Surface Polysialylation. *Nat Struct Mol Biol* **2015**, *22* (8), 627-35 DOI: 10.1038/nsmb.3060.

15. Lee, H. J.; Lairson, L. L.; Rich, J. R.; Lameignere, E.; Wakarchuk, W. W.; Withers, S. G.; Strynadka, N. C., Structural and Kinetic Analysis of Substrate Binding to the Sialyltransferase Cst-II from Campylobacter Jejuni. *J Biol Chem* **2011**, *286* (41), 35922-32 DOI: 10.1074/jbc.M111.261172.

16. Chiu, C. P.; Lairson, L. L.; Gilbert, M.; Wakarchuk, W. W.; Withers, S. G.; Strynadka, N. C., Structural Analysis of the α-2,3-sialyltransferase Cst-I from Campylobacter jejuni in Apo and Substrate-Analogue Bound Forms. *Biochemistry* **2007**, *46* (24), 7196-204 DOI: 10.1021/bi602543d.

17. Iwatani, T.; Okino, N.; Sakakura, M.; Kajiwara, H.; Takakura, Y.; Kimura, M.; Ito, M.; Yamamoto, T.; Kakuta, Y., Crystal Structure of α/β-Galactoside α2,3-Sialyltransferase from a Luminous Marine Bacterium, Photobacterium Phosphoreum. *FEBS Letters* **2009**, *583* (12), 2083-2087 DOI: 10.1016/j.febslet.2009.05.032.

18. Kim, D. U.; Yoo, J. H.; Lee, Y. J.; Kim, K. S.; Cho, H. S., Structural analysis of sialyltransferase PM0188 from Pasteurella multocida complexed with donor analogue and acceptor sugar. *BMB Rep* **2008**, *41* (1), 48-54 DOI.

19. Ni, L.; Chokhawala, H. A.; Cao, H.; Henning, R.; Ng, L.; Huang, S.; Yu, H.; Chen, X.; Fisher, A. J., Crystal structures of Pasteurella Multocida Sialyltransferase Complexes with Acceptor and Donor Analogues Reveal Substrate Binding Sites and Catalytic Mechanism. *Biochemistry* **2007**, *46* (21), 6288-98 DOI: 10.1021/bi700346w.

20. Sugiarto, G.; Lau, K.; Qu, J.; Li, Y.; Lim, S.; Mu, S.; Ames, J. B.; Fisher, A. J.; Chen, X., A Sialyltransferase Mutant with Decreased Donor Hydrolysis and Reduced Sialidase Activities for Directly Sialylating LewisX. *ACS Chem Biol* **2012**, *7* (7), 1232-40 DOI: 10.1021/cb300125k.

21. Huynh, N.; Li, Y.; Yu, H.; Huang, S.; Lau, K.; Chen, X.; Fisher, A. J., Crystal Structures of Sialyltransferase from Photobacterium Damselae. *FEBS Lett* **2014**, *588* (24), 4720-9 DOI: 10.1016/j.febslet.2014.11.003.

22. Schmolzer, K.; Czabany, T.; Luley-Goedl, C.; Pavkov-Keller, T.; Ribitsch, D.; Schwab, H.; Gruber, K.; Weber, H.; Nidetzky, B., Complete Switch from α-2,3- to α-2,6-Regioselectivity in Pasteurella Dagmatis β-D-Galactoside Sialyltransferase by Active-Site Redesign. *Chem Commun* **2015**, *51* (15), 3083-6 DOI: 10.1039/c4cc09772f.

23. Rao, F. V.; Rich, J. R.; Rakic, B.; Buddai, S.; Schwartz, M. F.; Johnson, K.; Bowe, C.; Wakarchuk, W. W.; Defrees, S.; Withers, S. G.; Strynadka, N. C., Structural Insight into

Mammalian Sialyltransferases. *Nat Struct Mol Biol* **2009**, *16* (11), 1186-8 DOI: 10.1038/nsmb.1685.

24. Meng, L.; Forouhar, F.; Thieker, D.; Gao, Z.; Ramiah, A.; Moniz, H.; Xiang, Y.; Seetharaman, J.; Milaninia, S.; Su, M.; Bridger, R.; Veillon, L.; Azadi, P.; Kornhaber, G.; Wells, L.; Montelione, G. T.; Woods, R. J.; Tong, L.; Moremen, K. W., Enzymatic Basis for N-glycan Sialylation: Structure of Rat α 2,6-Sialyltransferase (ST6GAL1) Reveals Conserved and Unique Features for Glycan Sialylation. *J Biol Chem* **2013**, *288* (48), 34680-98 DOI: 10.1074/jbc.M113.519041.

25. Volkers, G., Strynadka, N.C.J., PDB ID: 5CXY. *To be published* **2016**, DOI: 10.2210/pdb5cxy/pdb.

26. Müller, B.; Schaub, C.; Schmidt, R. R., Efficient Sialyltransferase Inhibitors Based on Transition-State Analogues of the Sialyl Donor. *Angewandte Chemie International Edition* **1998**, *37* (20), 2893-2897 DOI: 10.1002/(sici)1521-3773(19981102)37:20<2893::aid-anie2893>3.0.co;2-w.

27. Amann, F.; Schaub, C.; Müller, B.; Schmidt, R. R., New Potent Sialyltransferase Inhibitors—Synthesis of Donor and of Transition-State Analogues of Sialyl Donor CMP-Neu5Ac. *Chem Eur J* **1998**, *4* (6), 1106-1115 DOI: 10.1002/(sici)1521-3765(19980615)4:6<1106::aid-chem1106>3.0.co;2-7.

28. Schaub, C.; Muller, B.; Schmidt, R. R., New Sialyltransferase Inhibitors Based on CMP-Quinic Acid: Development of a New Sialyltransferase Assay. *Glycoconj J* **1998**, *15* (4), 345-54 DOI: 10.1023/A:1006917717161.

29. Schwörer, R.; Schmidt, R. R., Efficient Sialyltransferase Inhibitors Based on Glycosides of N-Acetylglucosamine. *J Am Chem Soc* **2002**, *124* (8), 1632-1637 DOI: 10.1021/ja017370n.

30. Skropeta, D.; Schworer, R.; Haag, T.; Schmidt, R. R., Asymmetric Synthesis and Affinity of Potent Sialyltransferase Inhibitors Based on Transition-State Analogues. *Glycoconj J* **2004**, *21* (5), 205-19 DOI: 10.1023/b:glyc.0000045093.96413.62.

31. Li, W.; Niu, Y.; Xiong, D.-C.; Cao, X.; Ye, X.-S., Highly Substituted Cyclopentane–CMP Conjugates as Potent Sialyltransferase Inhibitors. *J Med Chem* **2015**, *58* (20), 7972-7990 DOI: 10.1021/acs.jmedchem.5b01181.

32. Kumar, R.; Nasi, R.; Bhasin, M.; Huan Khieu, N.; Hsieh, M.; Gilbert, M.; Jarrell, H.; Zou, W.; Jennings, H. J., Sialyltransferase Inhibitors: Consideration of Molecular Shape and Charge/Hydrophobic Interactions. *Carbohydr Res* **2013**, *378*, 45-55 DOI: 10.1016/j.carres.2012.12.017.

33. Montgomery, A.; Szabo, R.; Skropeta, D.; Yu, H., Computational Characterisation of the Interactions Between Human ST6Gal I and Transition-State Analogue Inhibitors: Insights for Inhibitor Design. *J Mol Recognit* **2016**, *29* (5), 210-22 DOI: 10.1002/jmr.2520.

34. Montgomery, A. P.; Xiao, K.; Wang, X.; Skropeta, D.; Yu, H., Computational Glycobiology: Mechanistic Studies of Carbohydrate-Active Enzymes and Implication for Inhibitor Design. In *Adv. Protein Chem. Str.*, Academic Press: 2017.

35. Montgomery, A. P. S., Danielle; Yu, Haibo Transition state-based ST6Gal I inhibitors: Mimicking the phosphodiester linkage with a triazole or carbamate through an enthalpy-entropy compensation. **2017**, *In Press*.

36. Trott, O.; Olson, A. J., AutoDock Vina: Improving the Speed and Accuracy of Docking with a New Scoring Function, Efficient Optimization, and Multithreading. *J Comp Chem* **2010**, *31* (2), 455-61 DOI: 10.1002/jcc.21334.

37. Morris, G. M.; Huey, R.; Lindstrom, W.; Sanner, M. F.; Belew, R. K.; Goodsell, D. S.; Olson, A. J., AutoDock4 and AutoDockTools4: Automated Docking with Selective Receptor Flexibility. *J Comput Chem* **2009**, *30* (16), 2785-2791 DOI: 10.1002/jcc.21256.

38. Hanwell, M. D.; Curtis, D. E.; Lonie, D. C.; Vandermeersch, T.; Zurek, E.; Hutchison, G. R., Avogadro: an advanced semantic chemical editor, visualization, and analysis platform. *J Cheminform* **2012**, *4* (1), 1-17 DOI: 10.1186/1758-2946-4-17.

39. Humphrey, W.; Dalke, A.; Schulten, K., VMD: Visual Molecular Dynamics. *J Mol Graph* **1996**, *14* (1), 33-8, 27-8 DOI: 10.1016/0263-7855(96)00018-5.

40. Phillips, J. C.; Braun, R.; Wang, W.; Gumbart, J.; Tajkhorshid, E.; Villa, E.; Chipot, C.; Skeel, R. D.; Kale, L.; Schulten, K., Scalable Molecular Dynamics with NAMD. *J Comp Chem* **2005**, *26* (16), 1781-802 DOI: 10.1002/jcc.20289.

41. Best, R. B.; Zhu, X.; Shim, J.; Lopes, P. E. M.; Mittal, J.; Feig, M.; MacKerell, A. D., Optimization of the additive CHARMM all-atom protein force field targeting improved sampling of the backbone φ, ψ and side-chain χ(1) and χ(2) dihedral angles. *J Chem Theory Comput* **2012**, *8* (9), 3257-3273 DOI: 10.1021/ct300400x.

42. Vanommeslaeghe, K.; Hatcher, E.; Acharya, C.; Kundu, S.; Zhong, S.; Shim, J.; Darian, E.; Guvench, O.; Lopes, P.; Vorobyov, I.; Mackerell Jr, A. D., CHARMM General Force Field: A Force Field For Drug-Like Molecules Compatible with the CHARMM All-Atom Additive Biological Force Fields. *J Comput Chem* **2010**, *31* (4), 671-690 DOI: 10.1002/jcc.21367.

43. Huang, L.; Roux, B., Automated Force Field Parameterization for Non-Polarizable and Polarizable Atomic Models Based on Ab Initio Target Data. *J Chem Theory Comput* **2013**, *9* (8), DOI: 10.1021/ct4003477.

44. Yu, H. M., Andrew P.; Skropeta, Danielle, Force field parameters for transition state-based ST6Gal I inhibitors. **2017**, DOI: 10.6084/m9.figshare.5372788.v1.

45. Feller, S. E.; Zhang, Y.; Pastor, R. W.; Brooks, B. R., Constant Pressure Molecular Dynamics Simulation: The Langevin Piston Method. *J Chem Phys* **1995**, *103* (11), 4613-4621 DOI: 10.1063/1.470648.

46. Martyna, G. J.; Tobias, D. J.; Klein, M. L., Constant Pressure Molecular Dynamics Algorithms. *J Chem Phys* **1994**, *101* (5), 4177-4189 DOI: 10.1063/1.467468.

47. Darden, T.; York, D.; Pedersen, L., Particle Mesh Ewald: An N·log(N) Method for Ewald sums in Large Systems. *J Chem Phys* **1993**, *98* (12), 10089-10092 DOI: 10.1063/1.464397.

48. Andersen, H. C., Rattle: A "Velocity" Version of the Shake Algorithm for Molecular Dynamics Calculations. *J Comput Phys* **1983**, *52* (1), 24-34 DOI: 10.1016/0021-9991(83)90014-1.

49. Brooks, B. R.; Brooks III, C. L.; Mackerell Jr, A. D.; Nilsson, L.; Petrella, R. J.; Roux, B.; Won, Y.; Archontis, G.; Bartels, C.; Boresch, S.; Caflisch, A.; Caves, L.; Cui, Q.; Dinner, A. R.; Feig, M.; Fischer, S.; Gao, J.; Hodoscek, M.; Im, W.; Kuczera, K.; Lazaridis, T.; Ma, J.; Ovchinnikov, V.; Paci, E.; Pastor, R. W.; Post, C. B.; Pu, J. Z.; Schaefer, M.; Tidor, B.; Venable, R. M.; Woodcock, H. L.; Wu, X.; Yang, W.; York, D. M.; Karplus, M., CHARMM: The Biomolecular Simulation Program. *J Comput Chem* **2009**, *30* (10), 1545-1614 DOI: 10.1002/jcc.21287.

50. BIOVIA, D. S. *Discovery Studio Modelling Environment*, Dassault Systèmes: San Diego, **2016**.

51. Kyte, J.; Doolittle, R. F., A Simple Method for Displaying the Hydropathic Character of a Protein. *J Mol Biol* **1982**, *157* (1), 105-132 DOI: 10.1016/0022-2836(82)90515-0.

Table 1: Summary of MD simulations performed

Ligand	Simulation Name	Equilibrium steps (ns)	Free Simulation (ns)	Simulations Performed
None	APO	10	90	1
***(R)*-4**	CAR_R	10	90	3
***(S)*-4**	CAR_S	10	90	3
***(R)*-3**	LEAD_R	10	90	3
***(S)*-3**	LEAD_S	10	90	3
***(R)*-6**	TRI_R	10	90	3
***(S)*-6**	TRI_S	10	90	3

Table 2. Mean binding affinities against hST8Sia III of carbamate-linked ST inhibitors based on multiple docking calculations.

	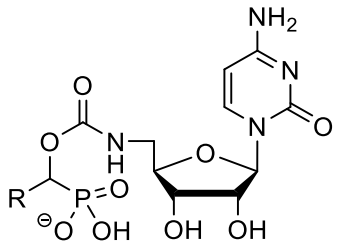		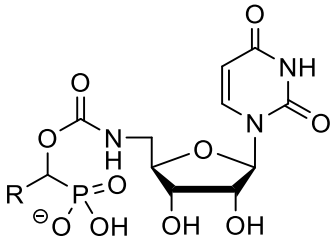	
R	**Cpd**	**Mean Binding Affinity (kcal/mol)[a]**	**Cpd**	**Mean Binding Affinity (kcal/mol)[a]**
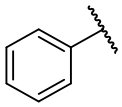	***(R)*-8** ***(S)*-8**	-9.5 ± 0.2 -9.3 ± 0.1	***(R)*-13** ***(S)*-13**	-9.5 ± 0.2 -9.5 ± 0.1
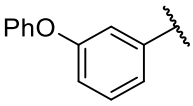	***(R)*-4** ***(S)*-4**	-10.5 ± 0.2 -10.4 ± 0.3	***(R)*-5** ***(S)*-5**	-10.7 ± 0.2 -10.3 ± 0.2
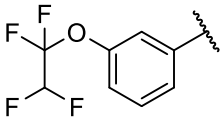	***(R)*-9** ***(R)*-9**	-10.0 ± 0.2 -10.0 ± 0.2	***(R)*-14** ***(R)*-14**	-10.1 ± 0.1 -10.1 ± 0.3
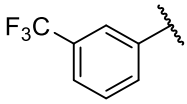	***(R)*-10** ***(S)*-10**	-9.9 ± 0.3 -9.7 ± 0.1	***(R)*-15** ***(S)*-15**	-10.0 ± 0.3 -9.9 ± 0.1
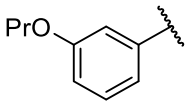	***(R)*-11** ***(S)*-11**	-9.5 ± 0.1 -9.3 ± 0.1	***(R)*-16** ***(S)*-16**	-9.5 ± 0.1 -9.5 ± 0.2
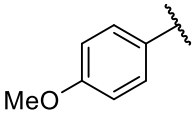	***(R)*-12** ***(S)*-12**	-9.4 ± 0.1 -9.3 ± 0.2	***(R)*-17** ***(S)*-17**	-9.4 ± 0.2 -9.4 ± 0.2

[a]Arithmetic mean of binding affinity ± SEM obtained from docking into six snapshots of the CAR_R1 simulation.

Table 3. Mean binding affinities against hST8Sia III of 1,2,3-triazole-linked ST inhibitors, based on multiple docking calculations.

	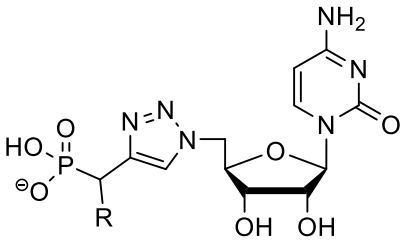		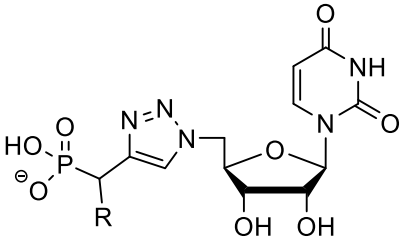	
R	**Cpd**	**Mean Binding Affinity (kcal/mol)[a]**	**Cpd**	**Mean Binding Affinity (kcal/mol)[a]**
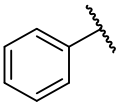	***(R)*-18** ***(S)*-18**	-9.8 ± 0.1 -10.1 ± 0.2	***(R)*-23** ***(S)*-23**	-10.0 ± 0.1 -9.7 ± 0.3
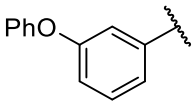	***(R)*-6** ***(S)*-6**	-10.9 ± 0.3 -11.0 ± 0.3	***(R)*-7** ***(S)*-7**	-10.8 ± 0.2 -11.0 ± 0.3
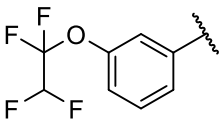	***(R)*-19** ***(S)*-19**	-10.1 ± 0.2 -10.5 ± 0.2	***(R)*-24** ***(S)*-24**	-10.3 ± 0.2 -10.6 ± 0.2
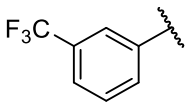	***(R)*-20** ***(S)*-20**	-10.2 ± 0.2 -10.6 ± 0.3	***(R)*-25** ***(S)*-25**	-10.1 ± 0.2 -10.5 ± 0.2
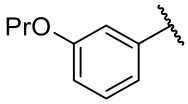	***(R)*-21** ***(S)*-21**	-9.4 ± 0.1 -9.9 ± 0.2	***(R)*-26** ***(S)*-26**	-9.7 ± 0.1 -10.2 ± 0.2
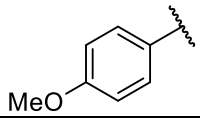	***(R)*-22** ***(S)*-22**	-9.8 ± 0.1 -10.0 ± 0.2	***(R)*-27** ***(S)*-27**	-9.7 ± 0.1 -10.1 ± 0.2

[a]Arithmetic mean of binding affinity ± SEM obtained from docking into six snapshots of the CAR_R1 simulation.

Table 4. Mean binding affinities against hST8Sia III of phosphodiester-linked ST inhibitors, based on multiple docking calculations.

	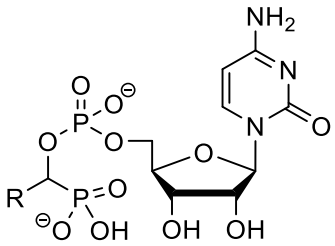		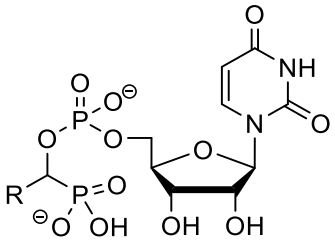	
R	**Cpd**	**Mean Binding Affinity (kcal/mol)[a]**	**Cpd**	**Mean Binding Affinity (kcal/mol)[a]**
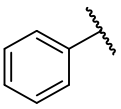	***(R)*-28** ***(S)*-28**	-9.3 ± 0.1 -9.3 ± 0.2	***(R)*-33** ***(S)*-33**	-9.3 ± 0.2 -9.4 ± 0.1
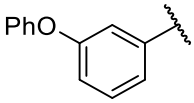	***(R)*-3** ***(S)*-3**	-10.2 ± 0.3 -10.3 ± 0.2	***(R)*-34** ***(S)*-34**	-10.3 ± 0.3 -10.3 ± 0.2
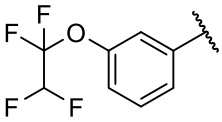	***(R)*-29** ***(S)*-29**	-9.7 ± 0.2 -9.8 ± 0.3	***(R)*-35** ***(S)*-35**	-10.0 ± 0.2 -10.1 ± 0.3
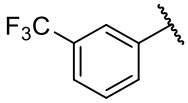	***(R)*-30** ***(S)*-30**	-9.8 ± 0.1 -9.9 ± 0.1	***(R)*-36** ***(S)*-36**	-9.8 ± 0.2 -9.8 ± 0.2
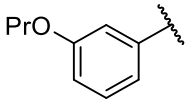	***(R)*-31** ***(S)*-31**	-9.2 ± 0.2 -9.4 ± 0.2	***(R)*-37** ***(S)*-37**	-9.3 ± 0.1 -9.5 ± 0.2
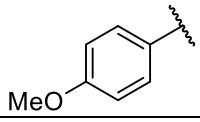	***(R)*-32** ***(S)*-32**	-9.2 ± 0.1 -9.3 ± 0.1	***(R)*-38** ***(S)*-38**	-9.3 ± 0.1 -9.4 ± 0.2

[a]Arithmetic mean of binding affinity ± SEM obtained from docking into six snapshots of the CAR_R1 simulation.

Table 5: Mean binding affinities against hST8Sia III of potential ST inhibitors with 2′ substitutions

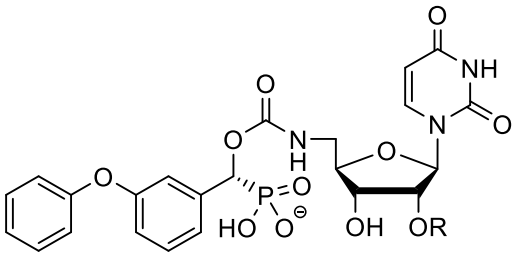

R	Cpd	Mean Binding Affinity (kcal/mol)[a]
H	***(R)*-5**	-10.7 ± 0.2
Me	***(R)*-39**	-10.9 ± 0.3
Et	***(R)*-40**	-10.6 ± 0.2
Pr	***(R)*-41**	-10.2 ± 0.2
CF_3	***(R)*-42**	-10.3 ± 0.2
CH_2CF_3	***(R)*-43**	-10.8 ± 0.2
C_6H_5	***(R)*-44**	Not accommodated

[a]Arithmetic mean of binding affinity ± SEM obtained from docking into six snapshots of the CAR_R1 simulation.

ChemDraw Figures

Figure 2:

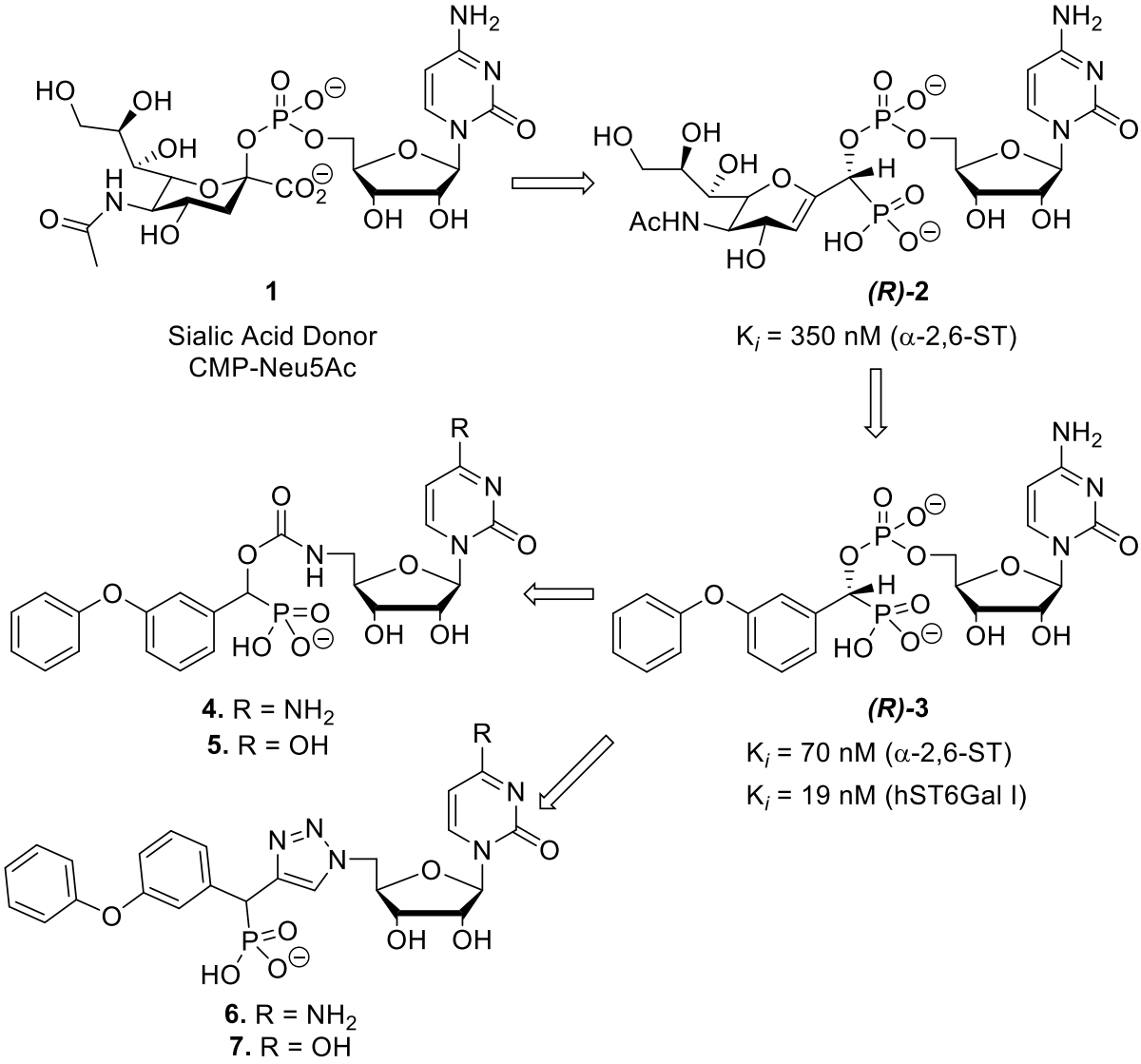

Figure 6:

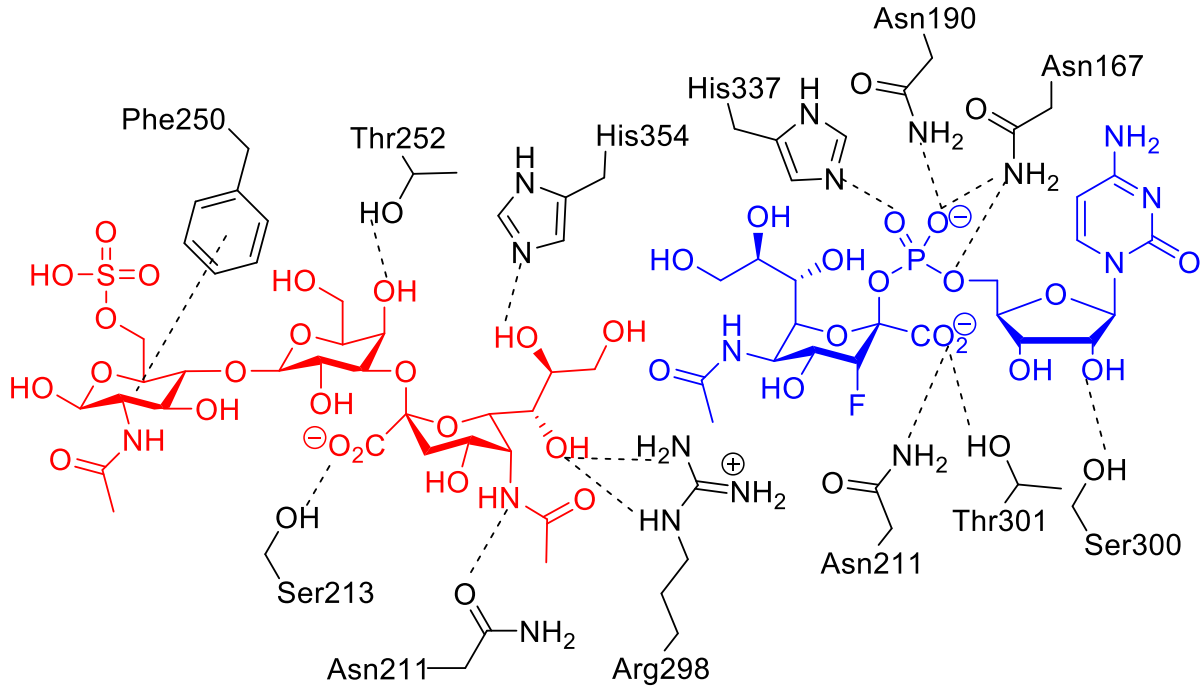

Figure 7:

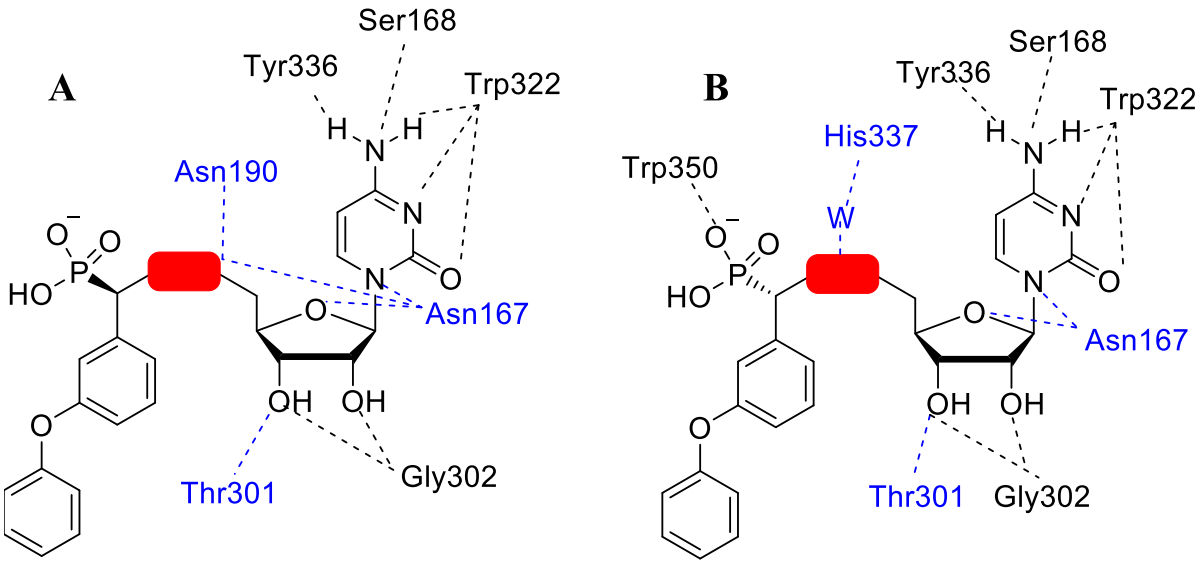

Figure 8:

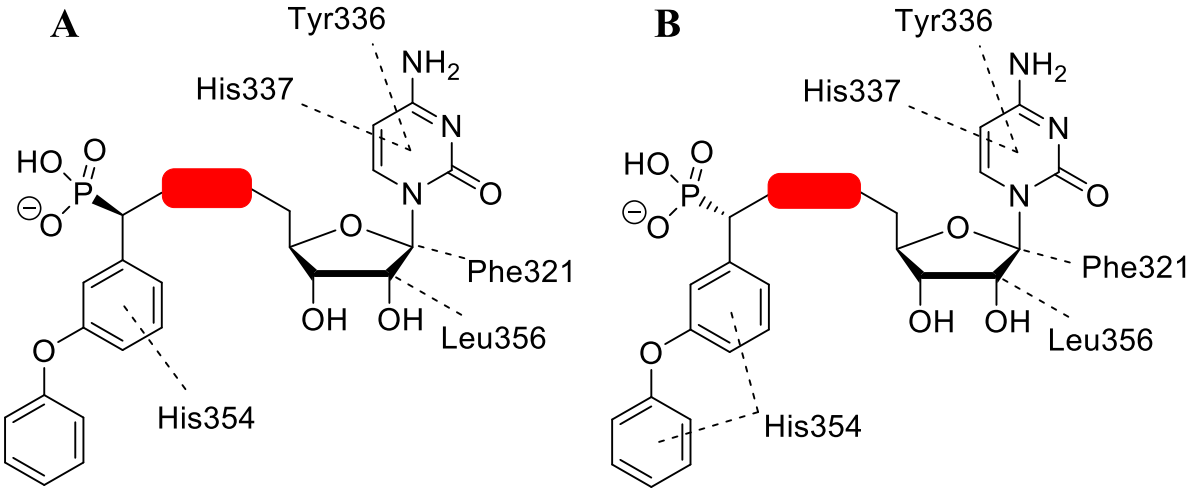

Figure 9:

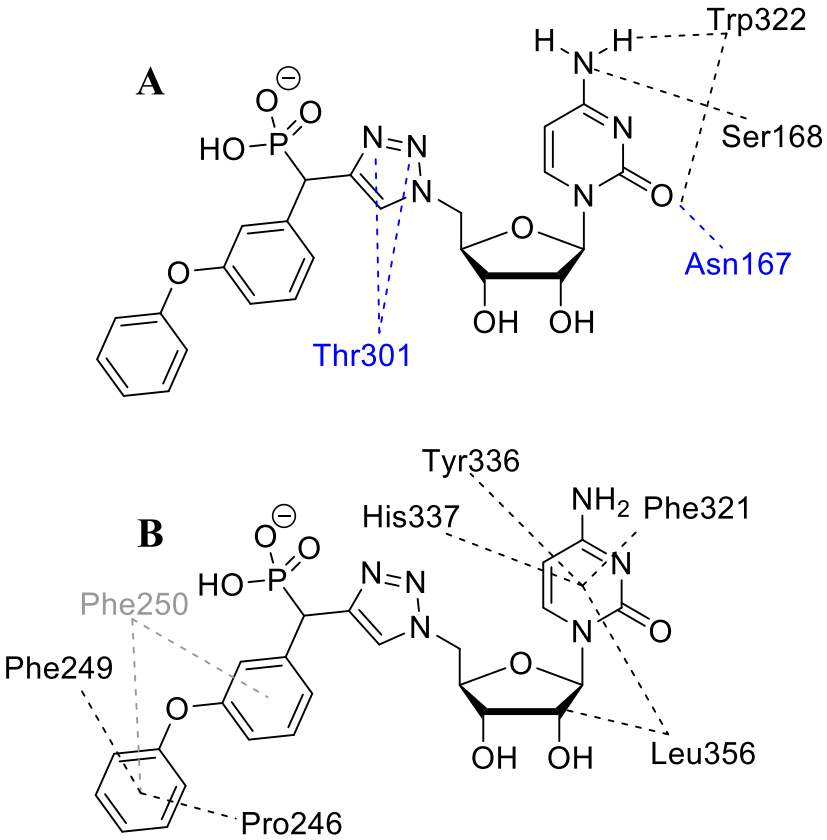

Figure Legends

Figure 1: The structure of hST8Sia III (PDB id:5CXY)[25], which was crystallised with the ligand 55T (blue). The soluble catalytic domain of hST8Sia III extends into the lumen of the Golgi apparatus via a stem region from a transmembrane domain (TMD) and a short *N*-terminal cytoplasmic domain. The flexible active-site loop (residues 341-354) is coloured in red.

Figure 2: Development of ST transition-state analogue inhibitors, from the one of the earliest (**2**),[29] to the most potent inhibitor to date (**3**),[30-31] which serves as our lead. Comparisons of carbamate (**4** and **5**), and 1,2,3-triazole (**6** and **7**) derivatives with the lead compound will be the focus of this study.

Figure 3: Comparison between the donor binding sites of pST3Gal I (left - bound to CMP; PDB id: 2WNB),[23] hST6Gal I (centre - bound to CMP; PDB id: 4JS2),[7] and hST8Sia III (right - bound to 55T; PDB id: 5CXY),[25] with the surface showing the hydrophobicity of the binding pocket, calculated according to the method of Kyte and Doolittle.[51]

Figure 4: Cα RMSFs of hST8Sia III, calculated for each MD simulation. Expanded figures are in supplementary information (Figures S14-S16).

Figure 5: (**A**) Comparison between the predicted binding modes of the *m*-phenoxy cytidine compound ***(R)*-4** (green) and the analogous uridine compound ***(R)*-5** (orange). (**B**); Comparison of binding conformations of the sialyl mimic of inhibitor ***(R)*-4**, with the orange conformation being the most common. The green binding mode gave generally higher binding affinity, with lower frequency, while the pink mode was the least frequently suggested by the docking procedure.

Figure 6: Significant non-bonded interactions described by Volkers *et al.*[14] of the donor and acceptor analogues CMP-3FNeu5Ac and Sia-6S-LacNAc respectively, with hST8Sia III. Some bonding interactions involving the protein backbone and the cytidine ring of CMP-3FNeu5Ac are not displayed.

Figure 7: Significant hydrogen bonding interactions of the (**A**) *R* and (**B**) *S* stereoisomers of the carbamate (CAR) and phosphodiester (LED) compounds with hST8Sia III across 90 ns of simulation. Blue residues denote those interactions which were also observed in the crystal structure. The red box represents the two linkers. Full interaction data shown in Tables S18, S20, S22, and S24.

Figure 8: Significant hydrophobic interactions of the (**A**) *R* and (**B**) *S* stereoisomers of the CAR and LED simulations with hST8Sia III across 90 ns of simulation. The red box represents the two linkers. Full interaction data shown in Tables S19, S21, S23, and S25.

Figure 9: Significant non-bonded interactions of triazole (TRI) with hST8Sia III across 90ns of free simulation in each of the six triazole (TRI) simulations. **(A)** Hydrogen bond analysis (blue residues denote those interactions which were also observed in the crystal structure), **(B)** hydrophobic contacts (grey residues denote interactions which were consistent in simulations of one stereoisomer). Full interaction data is shown in Supplementary Tables S26-S29.